J. Mod. Power Syst. Clean Energy (2014) 2(1):16–22
DOI 10.1007/s40565-014-0051-5

Robust current control design of a three phase voltage source converter

Wenming GONG, Shuju HU (✉), Martin SHAN, Honghua XU

Abstract In this paper, a robust design method for current control is proposed to improve the performance of a three phase voltage source converter (VSC) with an inductor-capacitor-inductor (LCL) filter. The presence of the LCL filter complicates the dynamics of the control system and limits the achievable control bandwidth (and the overall performance), particularly when the uncertainty of the parameters is considered. To solve this problem, the advanced H∞ control theory is employed to design a robust current controller in stationary coordinates. Both control of the fundamental frequency current and suppression of the potential LC resonance are considered. The design procedure and the selection of the weight functions are presented in detail. A conventional proportional-resonant PR controller is also designed for comparison. Analysis showed that the proposed H∞ current controller achieved a good frequency response with explicit robustness. The conclusion was verified on a 5 kW VSC that had a LCL filter.

Keywords Current control, H∞ control, Robust control, Inductor-capacitor-inductor (LCL) filter, Voltage source converter (VSC)

Received: 31 December 2013 / Accepted: 11 March 2014 / Published online: 23 March 2014

W. GONG, University of Chinese Academy of Sciences, Beijing 100190, China
e-mail: gwm@mail.iee.ac.cn
S. HU, H. XU, Institute of Electrical Engineering, Chinese Academy of Sciences, Beijing 100190, China
(✉) e-mail: hushuju@mail.iee.ac.cn
H. XU
e-mail: hxu@mail.iee.ac.cn
M. SHAN, Control Engineering and Energy Storage Systems, Fraunhofer IWES, 34119 Kassel, Germany
e-mail: martin.shan@iwes.fraunhofer.de

1 Introduction

With the use of a pulse width modulation (PWM) technique, the voltage source converter (VSC) had excellent P&Q operation characteristics, which is shown in Fig. 1. VSCs have been widely used in renewable energy production, smart grids, uninterruptable power supplies (UPSs), active power filtering (APF), and electrical drives [1]. With the development of self-commutated power electronic devices, the capacity of VSCs have been sustained with their growth. The state of the art of this technology is its application in VSC-HVDC systems [2, 3].

In high power applications, a LCL filter is usually employed to filter out the PWM switching frequency components. Compared with the L filter of a single inductor, the LCL filter is much smaller in weight and size, but has a similar low frequency performance. Therefore, the LCL filter is a better choice in this context because it allows for the use of a lower switching frequency that meets the harmonic limits and further decreases the switching losses [4, 5].

A critical innate problem that the LCL filters have is a low damped LC resonance. Resistors can be simply used to provide passive damping to the resonance. However, this has the disadvantage of an increased power loss [6]. Several active damping control strategies have been suggested, such as lead-lag compensation [7] and virtual resistance [8, 9]. However, these control methods usually limit the control bandwidth. There is a tradeoff between the closed loop performance and the system stability. In addition, the uncertainty in the grid environment worsens this problem. Grid operation, cable overload, saturation, and temperature effects can cause variations in the interfacing impedance and the resonance frequency, which makes the control design much more difficult [10].

To enhance the performance of a VSC with all these restrictions, the H∞ control theory was applied to design a

STATE GRID
STATE GRID ELECTRIC POWER RESEARCH INSTITUTE

robust current controller for the VSC system in stationary coordinates in this paper. The H∞ control theory dealing with the model and disturbance uncertainty. This is a relatively new method for the controller design of VSCs. However, there are still several successful examples. In [11], the authors developed a tuning strategy for designing multiple-loop lag-lead compensators for uninterruptable power supplies (UPSs) based on the H∞ robust control theory. The H∞ tuned compensator was asymptotically stable with guaranteed performance. In [12], a robust control scheme with an outer H∞ voltage control loop and an inner current control loop was designed for a dynamic voltage restorer (DVR). The H∞ voltage controller was effective in both balanced and unbalanced sag compensation as well as load disturbance rejection. In [13], a H∞ current controller was designed for a grid connected to a power factor correction (PFC). It was possible to explicitly specify the degree of robustness with variations in the parameters using the proposed method. A mixed-sensitivity method was used to synthesize the H∞ controller. A high pass weight function was used to guarantee a robust performance and to avoid possible oscillations caused by the capacitor connected in parallel. However, none of the previous works focused on VSCs with an LCL filter. In this paper the H∞ method is further developed; the ability to achieve LC resonance attenuation is enhanced. Alternatively, from the previous work, the LC resonance in this paper is modeled as a noise channel and the corresponding weight functions are proposed to provide a robust performance.

The remainder of this paper is organized as follows: in Section 2, the system model is introduced and the problem with the LC resonance is described. In Section 3, the design procedure of the proposed H∞ current controller and the selection of weight functions are presented. A conventional PR controller is also designed for comparison. The performance is then analyzed in detail. In Section 4, the experimental results are explained. Finally, conclusions are given in Section 5.

2 System modelling

2.1 Mathematical model of the VSC system

As shown in Fig. 1, the studied VSC was connected to the grid via the LCL interface. R_c and L_c are the resistance and inductance for the inductor of the converter side, respectively; R_g and L_g represent the equivalent resistance and inductance for the inductor of the grid side and the AC grid line impedance, respectively; C_f is the filter capacitor; C_{dc} is the DC capacitor; u_g is the grid voltage; u_f is the filter capacitor voltage; i_g is the injected grid current; i_c is the converter output current; u_c is the converter output voltage; u_{dc} is the DC capacitor; and i_{dc} is the DC load current.

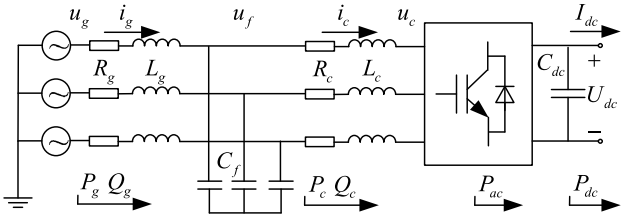

Fig. 1 The grid connected voltage source converter

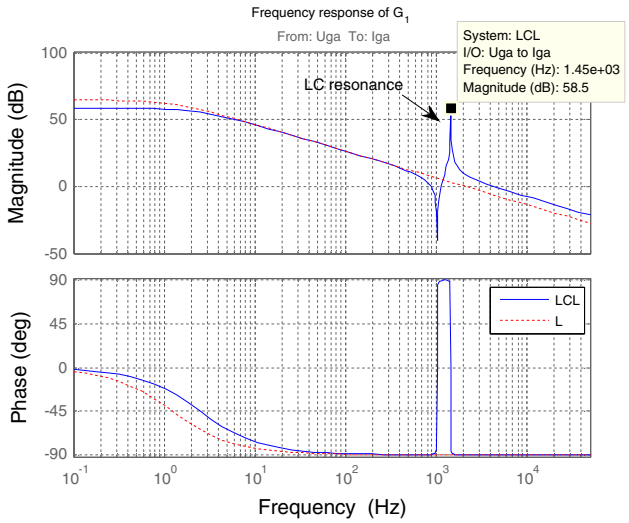

Fig. 2 Frequency response of the open loop system of a VSC

In stationary α-β coordinates, the per-phase mathematic model of the AC side can be written as:

$$\begin{cases} L_g \frac{\mathrm{d}i_g}{\mathrm{d}t} = -R_g i_g + u_g - u_f \\ C_f \frac{\mathrm{d}u_f}{\mathrm{d}t} = i_g - i_c \\ L_c \frac{\mathrm{d}i_c}{\mathrm{d}t} = -R_c i_c + u_f - u_c. \end{cases} \tag{1}$$

On the DC side the model can be written as,

$$C_{dc} \frac{\mathrm{d}U_{dc}}{\mathrm{d}t} = \frac{P_{ac}}{U_{dc}} - I_{dc} = \frac{3(u_{c\alpha} i_{c\alpha} + u_{c\beta} i_{c\beta})}{2U_{dc}} - I_{dc}. \tag{2}$$

The values for the parameters are shown in Appendix A. The impedance of the AC grid line was uncertain. In addition, taking into consideration of the measurement error and nonlinear characteristics, ±50% uncertainty in all of the parameters were reasonable for robust analysis.

2.2 LC resonance

From (1), the transfer function of the AC side was derived as:

$$i_g = G_1 u_g + G_2 u_c. \tag{3}$$

The frequency response of G_1 is depicted in Fig. 2. The response is similar to that of G_2. For comparison, a system that used a common single L ($L_g + L_c$) filter is also

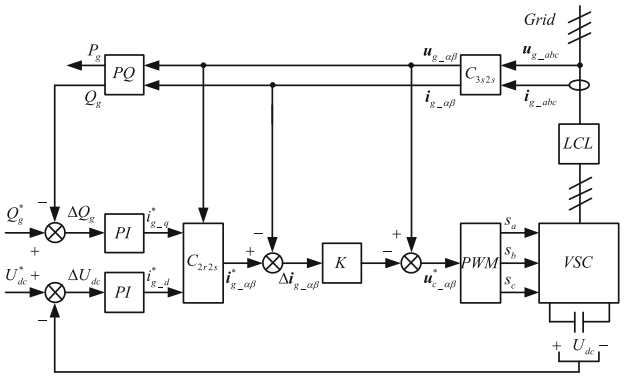

Fig. 3 Multiloop vector control scheme of a VSC

depicted. In the low frequency region, the two systems were similar to each other, which implied that there was a similar control design for the fundamental components. In the high frequency region, there was a single resonance peak with the LCL filter, which can be modeled as noise from the feedback system. The resonance frequency was about 1.45 kHz, which was calculated using:

$$f_{res} = \frac{\omega_{res}}{2\pi} = \frac{1}{2\pi}\sqrt{\frac{L_g + L_c}{L_g L_c C_f}}. \tag{4}$$

The LC resonance, which was caused by the LCL filter, needs to be dampened properly, otherwise the system will become unstable. Uncertainties in the system parameters can make the resonance frequency difficult to identify. In the next section, both the control design of the fundamental components and the suppression of the LC resonance are discussed.

3 Control design

3.1 Multi-loop control scheme

In most applications, a multi-loop vector control scheme, either in stationary or rotating coordinates, is adopted to improve the transient and steady-state performances [1]. The inner current loop is responsible for the overall stability of the system and for attenuating the LC resonance introduced by the filter. The outer loop is usually much slower than the inner loop.

In this paper, the outer loop was used to control the DC voltage and the output reactive power, as shown in Fig. 3. Meanwhile, the inner current loop was designed in stationary coordinates. The injected grid current was fed back into the system for ease of controlling the reactive power.

For coordinate transformations, the C_{3s2s} and C_{2r2s} blocks are:

$$C_{3s2s}: \begin{bmatrix} u_{g\_\alpha} \\ u_{g\_\beta} \end{bmatrix} = \begin{bmatrix} 1 & -\frac{1}{2} & -\frac{1}{2} \\ 0 & \frac{\sqrt{3}}{2} & -\frac{\sqrt{3}}{2} \end{bmatrix} \begin{bmatrix} u_{g\_a} \\ u_{g\_b} \\ u_{g\_c} \end{bmatrix}$$
$$\begin{bmatrix} i_{g\_\alpha} \\ i_{g\_\beta} \end{bmatrix} = \begin{bmatrix} 1 & -\frac{1}{2} & -\frac{1}{2} \\ 0 & \frac{\sqrt{3}}{2} & -\frac{\sqrt{3}}{2} \end{bmatrix} \begin{bmatrix} i_{g\_a} \\ i_{g\_b} \\ i_{g\_c} \end{bmatrix}, \tag{5}$$

$$C_{2r2s}: \begin{bmatrix} i^*_{g\_\alpha} \\ i^*_{g\_\beta} \end{bmatrix} = \frac{1}{u^2_{g\_\alpha} + u^2_{g\_\beta}} \begin{bmatrix} u_{g\_\alpha} & -u_{g\_\beta} \\ u_{g\_\beta} & u_{g\_\alpha} \end{bmatrix} \begin{bmatrix} i^*_{g\_d} \\ i^*_{g\_q} \end{bmatrix}. \tag{6}$$

The PQ block was used to calculate active and reactive power:

$$PQ: \begin{bmatrix} P_g \\ Q_g \end{bmatrix} = \begin{bmatrix} u_{g\_\alpha} & u_{g\_\beta} \\ u_{g\_\beta} & -u_{g\_\alpha} \end{bmatrix} \begin{bmatrix} i_{g\_\alpha} \\ i_{g\_\beta} \end{bmatrix}. \tag{7}$$

3.2 PR current control design

In stationary coordinates, a PR controller is usually used to track the sinusoidal signals. In this paper, a PR controller was used for comparison.

$$K = \left(k_p + \frac{2k_i\omega_c s}{s^2 + 2\omega_c s + \omega_n^2}\right) \begin{bmatrix} 1 & 0 \\ 0 & 1 \end{bmatrix}, \tag{8}$$

where k_p and k_i are gain constants; ω_c is the cut-off frequency and $\omega_n = 100\pi$ for a 50 Hz system. More details of the control design can be found in [14].

3.3 H∞ current control design

The PR controller has been successfully used in many VSC systems. However, further improvements in its performance are limited by the presence of the LC resonance.

The advanced H∞ control theory was employed in this section in the current control design. The overall performance was specified by choosing proper weight functions. The controller was then calculated by solving the algebraic Riccati functions [15]. The order of the synthesized controller was equal to the sum of the controlled plant and the weight functions.

A diagram of the control design is shown in Fig. 4, where G_1 and G_2 are the same as in (3). W_p, W_u and W_n are the performance, control and noise weight functions, respectively. As can be seen in Fig. 2, L and LCL had similar frequency responses near the fundamental frequency. Therefore, an L filter model could be used to control the fundamental frequency components by reducing the order of the final controller. The LC resonance, which was caused by the LCL filter, was considered as noise. This is a new development for the design of a VSC control and it is sensible and effective, according to the experimental results.

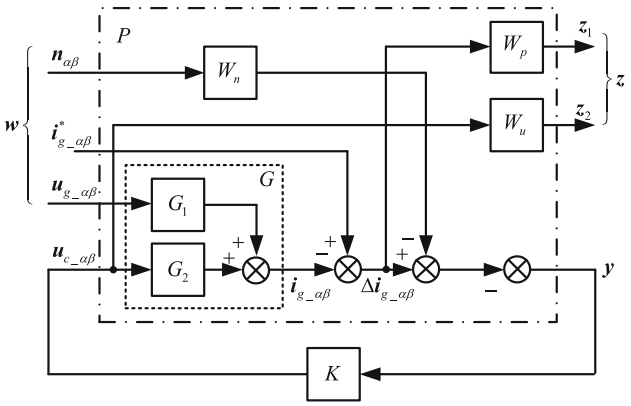

Fig. 4 Diagram of the H∞ current control design

In this mixed H∞ problem, the control design aimed to obtain a stable controller that minimized the H∞ norm of the generalized transfer function (P) from w to z as shown in Fig. 4.

$$\left\| \begin{matrix} W_p S_o & -W_p S_o G_1 & W_p S_o G_2 K W_n \\ W_u S_i K & -W_u S_i K G_1 & -W_u S_i K W_n \end{matrix} \right\| < \gamma, \tag{9}$$

where $S_i = (I + KG_2)^{-1}$ and $S_o = (I + G_2K)^{-1}$ are the input and output sensitivity transfer functions, respectively, and γ is the peak value of the H∞ norm. For $\gamma < 1$, the system was robust stable within the desired uncertainty range.

From (6), the closed loop performance of the system was largely dependent on the shape of the weight functions. To prevent the control signal from being too large, $W_u = 1$ was chosen for the scaled signals. The other two weight functions were related to the tracking performance and the robust stability.

3.3.1 *Performance weight function*

The sensitivity function, S, is an indication of the tracking performance of the system. As such, the weight function (W_p) can be used to specify the control performance [15]. As shown in Fig. 3, the current reference is a sinusoidal signal in α-β coordinates. Thus, S should be as small as possible at the fundamental frequency. For the sinusoidal signal, a second order resonant filter was adopted:

$$W_p = \frac{k_n \omega_n^2}{s^2 + 2\zeta_n \omega_n s + \omega_n^2} \begin{bmatrix} 1 & 0 \\ 0 & 1 \end{bmatrix}, \tag{10}$$

where ω_n, k_n and ζ_n are the fundamental frequency,the gain constant and the damping ratio, respectively.

3.3.2 *Noise weight function*

To improve the robust stability and suppress the LC resonance, a proper noise weight function needs to be

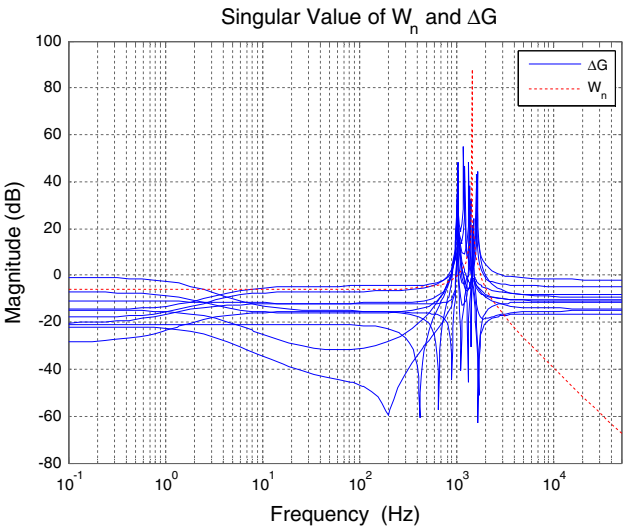

Fig. 5 Frequency response of the open loop system

defined. The variations in the model can be measured using a singular input-output value [16].

$$\Delta(G) = \sigma_{\max}\left(\frac{G_P - G_N}{G_N}\right), \tag{11}$$

where G_N is the nominal plant and G_P is the disturbed plant.

From Fig. 5, the variation in the circuit parameters caused a large uncertainty near the resonance frequency. There was only one resonance peak in the LCL filter. Thus, a second order resonant filter can be used to model the LC resonance a noise:

$$W_n = \frac{k_{res} \omega_{res}^2}{s^2 + 2\zeta_{res} \omega_{res} s + \omega_{res}^2} \begin{bmatrix} 1 & 0 \\ 0 & 1 \end{bmatrix}, \tag{12}$$

where ω_{res}, k_{res} and ζ_{res} are the resonant frequency, the gain constant and the damping ratio, respectively.

3.4 Design results

Here, one PR controller and two types of H∞ controllers are compared. PR is a conventional control, for comparison. H∞(I) is a basic H∞ control. Only W_u and W_p were used (W_n was removed). For H∞(II): W_u, W_p, and W_n were used at the same time to guarantee that the overall performance was robust.

An important step in the design of the H∞ control is loop-shaping, which is similar to the traditional Bode's response method, but can be applied to Multiple-Input Multiple-Output systems. First, the weight functions were designed. The controller was then synthesized by iterations, to reduce the H∞ norm. The frequency response could then be depicted. The frequency response of the weight functions covered the critical frequency, allowing

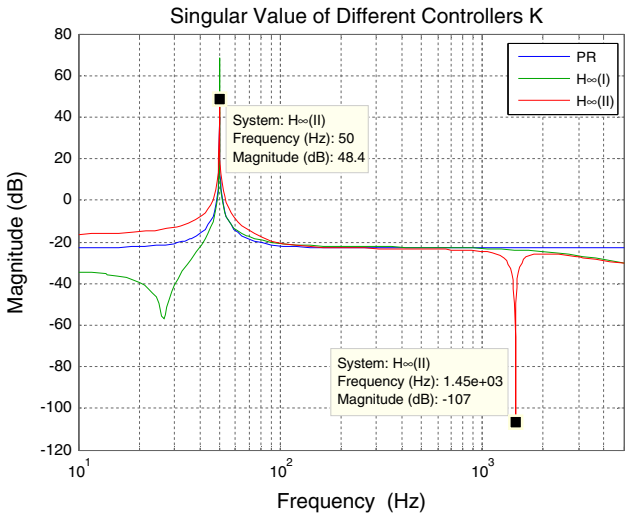

Fig. 6 The singular value of the controllers

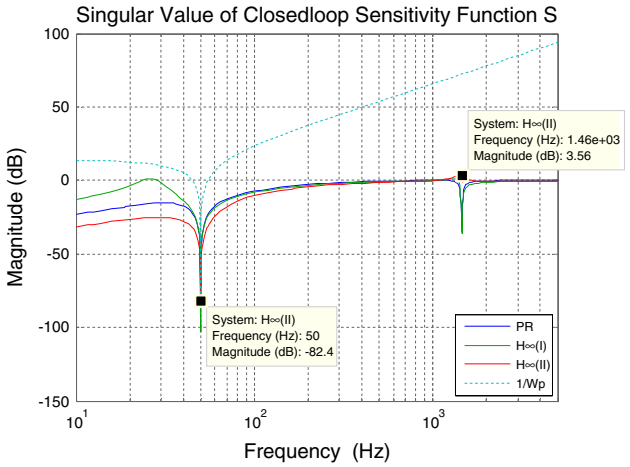

Fig. 7 The singular value of the sensitivity function, S

for a satisfactory stability and performance to be obtained. By checking the frequency response, weight functions can be redesigned or the parameters modified to obtain a more ideal shape.

In this paper, the parameters of the weight functions were tuned by loop-shaping of the T-S response. The circuit parameters and the tuned weight function parameters can be found in Appendix A. The H∞ controllers were synthesized with the robust control toolbox included in MATLAB. In all cases, a H∞ norm of $\gamma = 1.0046$ was achieved, indicating the robust stability of the designed uncertainty.

The singular values of the controllers are depicted in Fig. 6. For comparison, the controllers were tuned to have similar responses in the low frequency range.

The singular value of the closed loop sensitivity function (S) and complementary sensitivity function (T) are shown

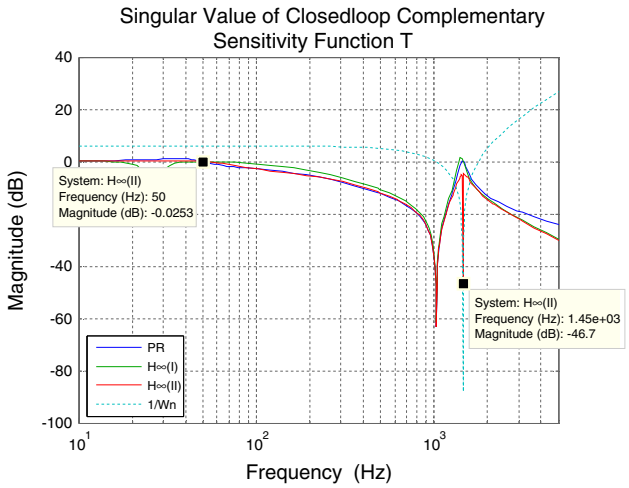

Fig. 8 The singular value of the complementary sensitivity function, T

Table 1 THDs (%) of the injected grid currents

Power (kVA)	1	2	3	4	5
PR	4.8	5.1	4.8	4.3	2.4
H∞(I)	4.7	4.7	4.2	3.7	2.6
H∞(II)	4.0	3.8	3.5	2.4	1.7
H∞(II$_2$)	4.2	3.9	3.6	2.6	1.7

in Figs. 7 and 8, respectively. In Fig. 7 the $\|S\|$ value was small around $f = 50$ Hz for all three controllers, which indicated that there was a small tracking error in the fundamental components. Thus, the three controllers were all capable for fundamental control of the current.

In Fig. 8, the H∞ controllers had a faster roll off speed than the PR controller in the high frequency range, which indicated that they had a better harmonic rejection ability. Because of the shaping effect of W_n, H∞(II) had a deep subsidence around the LC resonance frequency; while the other frequencies were not affected. This feature made the system much more stable and insensitive to LC resonance.

4 Experimental results

Experiments were carried out with all three of the controllers designed in Section 3.4. The experimental system included a 5 kW VSC with a LCL filter. The circuit parameters can be found in Appendix A. An additional type II controller with an incorrect resonance frequency (W_{n2}) was also designed to verify the robust performance of the system. System stability was guaranteed during the design of the controller.

The overall performance was evaluated by the total harmonic distortion (THD) of i_g, which is shown in

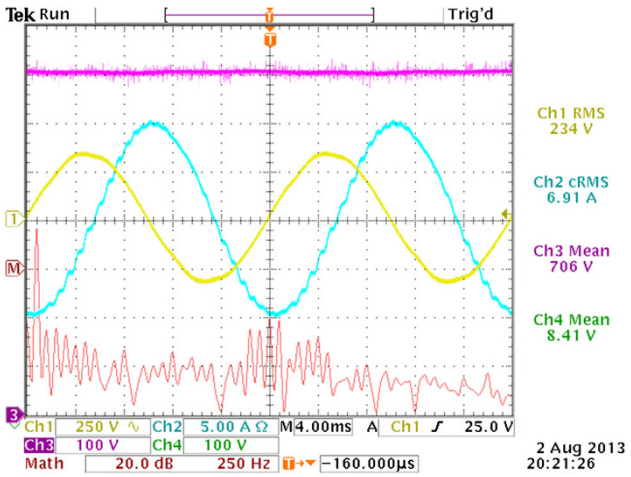

Fig. 9 Experiment results with PR controller

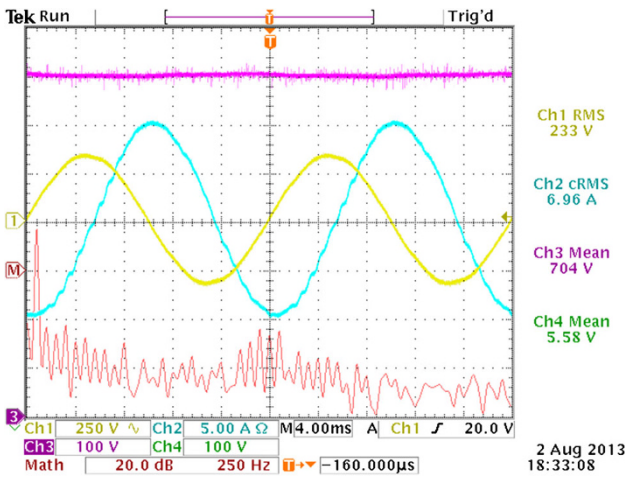

Fig. 10 Experiment results with H∞(I) controller

Table 1. The THD of the grid voltage was about 1.2%–1.4% during all of the experiments. A smaller THD for the output current resulted in a better performance of the controller.

From the measured THD, it was verified that all three controllers were capable of fulfilling the control requirements for the fundamental frequency components, in which the PR and H∞(I) controllers had similar performances owing to their similar frequency responses, as shown in Section 3.4. The H∞(II) controller had the best performance. Even with the incorrect parameters, the H∞(II) controller still achieved a relatively good result because of the deep subsidence around the LC resonance frequency, as shown in the singular response plots in Figs. 6, 7 and 8.

Three oscilloscope screenshots are given in Figs. 9, 10, and 11, in which, Ch1 is the grid voltage of phase a (u_{g_a}); Ch2 is the grid current of phase a (i_{g_a}); Ch3 is the DC side voltage (U_{dc}); Ch4 was not used; and ChM is the FFT analysis of Ch2. From these figures, the current with the H∞(II) controller (Fig. 11) was much smoother than those with the PR (Fig. 9) and H∞(I) (Fig. 10) controllers, and the FFT curve was less volatile around the LC resonance frequency.

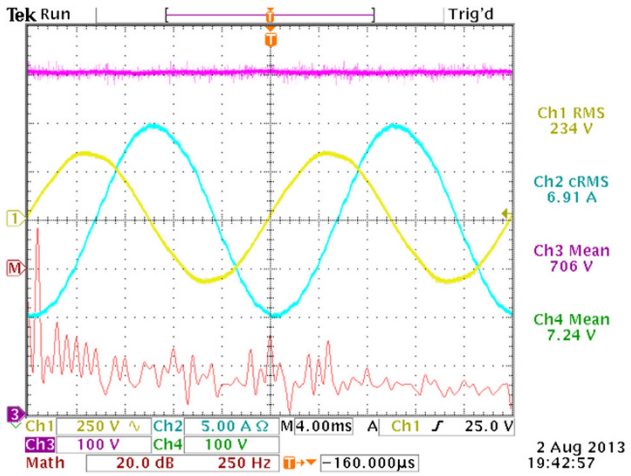

Fig. 11 Experiment results with H∞(II) controller

The LC resonance made the control bandwidth of the PR controller difficult to increase. The H∞(II) controller successfully suppressed the LC resonance and was less sensitive to variations in the parameters than the PR controller, i.e. the H∞(II) controller became more robust in terms of its stability and performance.

5 Conclusion

In this paper, a robust current control design method was proposed to enhance the performance of VSC systems with LCL filters, and the details on the design procedure were explained.

Based on the theoretical analysis and the experimental results, it can be concluded that the proposed H∞ current controller was capable of fundamental control of the frequency current and it potentially suppressed the LC resonance. The overall performance of the proposed H∞ current controller was better than that of a conventional PR controller. The H∞ controller was stable with certain parameter uncertainties and it was not sensitive to the LC resonance frequency. The unified H∞ control tools have proven to be effective for multivariable and multi-objective control designs in VSC applications.

Acknowledgments This research was supported by the CAS Fraunhofer Joint Doctoral Promotion Program (DPP) and the National High Technology Research and Development Program of China (863 program) (No. 2011AA050204).

Appendix A

System parameters:
$P_n = 5$ kW; $U_{line\_n} = 400$ V; $U_{DC\_n} = 700$ V; $f_n = 50$ Hz;
$R_g = R_c = 18 \times (1 \pm 50\%)$ mΩ; $L_g = L_c = 1.2 \times (1 \pm 50\%)$ mH;
and
$C_f = 20 \times (1 \pm 50\%)$ μF; $C_{dc} = 500$ μF.

PR controller:
$k_p = 0.07$; $k_i = 100$ and $\omega_c = 0.1$ rad/s.

Performance weight function:
W_p: $\omega_n = 50 \times 2\pi$ rad/s; $k_n = 0.06$ and $\zeta_n = 0.00001$.

Noise weight function:
W_n: $\omega_{res} = 1453 \times 2\pi$ rad/s; $k_{res} = 0.01$; $\zeta_{res} = 0.00001$;
W_{n2}: $\omega_{res} = 1250 \times 2\pi$ rad/s; $k_{res} = 0.01$; and $\zeta_{res} = 0.00001$.

References

[1] Wu B (2006) Hing-power converters and AC drives. Wiley, Hoboken
[2] Xu SK, Liang YY, Guo ZY (2011) Field commissioning test of CNOOC Wenchang VSC-HVDC transmission system. South Power Syst Technol 5(4):1–4 (in Chinese)
[3] Qiao WD, Mao YK (2011) Overview of Shanghai flexible HVDC transmission demonstration project. East China Electr Power 39(7):1137–1140 (in Chinese)
[4] Park SY, Chen CL, Lai JS et al (2008) Admittance compensation in current loop control for a grid-tie LCL fuel cell inverter. IEEE Trans Power Electron 23(4):1716–1723
[5] Jovcic D, Zhang L, Hajian M (2013) LCL VSC converter for high-power applications. IEEE Trans Power Deliver 28(1):137–144
[6] Peña-Alzola R, Liserre M, Blaabjerg F et al (2013) Analysis of the passive damping losses in LCL-filter-based grid converters. IEEE Trans Power Electron 28(6):2642–2646
[7] Blasko V, Kaura V (1997) A novel control to actively damp resonance in input LC filter of a three-phase voltage source converter. IEEE Trans Ind Appl 33(2):542–550
[8] Dahono PA (2003) A method to damp oscillations on the input LC filter of current-type AC-DC PWM converters by using a virtual resistor. In: Proceedings of the 25th international telecommunications energy conference (INTELEC'03), Yokohama, Japan, 19–23 Oct 2003, pp 757–761
[9] Wessels C, Dannehl J, Fuchs FW (2008) Active damping of LCL-filter resonance based on virtual resistor for PWM rectifiers—stability analysis with different filter parameters. In: Proceedings of the IEEE power electronics specialists conference (PESC'08), Rhodes, Greece, 15–19 Jun 2008, pp 3532–3538
[10] Mohamed YA-RI, A-Rahman M, Seethapathy R (2012) Robust line-voltage sensorless control and synchronization of LCL-filtered distributed generation inverters for high power quality grid connection. IEEE Trans Power Electron 27(1):87–98
[11] Willmann G, Coutinho DF, Pereira LFA et al (2007) Multiple-loop H-infinity control design for uninterruptible power supplies. IEEE Trans Ind Electron 54(3):1591–1602
[12] Li YW, Vilathgamuwa DM, Blaabjerg F et al (2007) A robust control scheme for medium-voltage-level DVR implementation. IEEE Trans Ind Electron 54(4):2249–2261
[13] Li YW, Vilathgamuwa DM, Loh PC (2007) Robust control scheme for a microgrid with PFC capacitor connected. IEEE Trans Ind Appl 43(5):1172–1182
[14] Teodorescu R, Blaabjerg F, Liserre M et al (2006) Proportional-resonant controllers and filters for grid-connected voltage-source converters. IEEE Xplore-Electr Power Appl 153(5):50–762
[15] Skogestad S, Postlethwaite I (2005) Multivariable feedback control: analysis and design. Wiley, Chichester
[16] Aten M, Werner H (2003) Robust multivariable control design for HVDC back to back schemes. IEEE Xplore-Gener Transm Distrib 150(6):761–767

Wenming GONG is now a Ph.D. candidate at University of Chinese Academy of Sciences. His research interests include the control of power electronics in wind energy and VSC-HVDC systems.

Shuju HU is an associate researcher at Institute of Electrical Engineering, Chinese Academy of Sciences. His research interests includes the control and test technologies of wind power systems and PV systems

Martin SHAN is head of Department Control Engineering, Fraunhofer IWES (Kassel). His research interests include modeling, simulation and control for wind turbines.

Honghua XU is a professor and research fellow at Institute of Electrical Engineering, Chinese Academy of Sciences. His research interests include wind power, photovoltaic and hybrid power system technologies.